

A Computer Model of Neural Processes Observed in the Cat Motor Cortex during Performance of an Operant Movement

V. I. Maiorov

UDC 612.014.3+612.829.3+612.825

Translated from Zhurnal Vysshei Nervnoi Deyatel'nosti, Vol. 52, No. 4, pp. 467–478, July–August, 2002. Original article submitted January 11, 2001, accepted May 30, 2001.

This report describes a computer model of a “column” in the cat motor cortex. The model includes two layers of two-segment pyramidal neurons with two groups of inhibitory interneurons in each layer, which selectively control the somatic and dendritic segments of the pyramidal cells. In this model, neurons include active sodium, calcium, and several types of potassium currents. Excitatory connections between neurons are of the AMPA and NMDA types, while collateral connections between neurons of the upper layer are mainly of the NMDA type; connections between neurons in the lower layer are of the AMPA type. All inhibitory connections are of the GABA_A type. The model reproduces the main neuronal processes seen in the cat motor cortex during performance of an operant movement. Pyramidal neurons of the upper layer generate primary and secondary responses to external stimuli. As in real experiments, secondary NMDA-dependent responses appear when GABA_A inhibition is weakened and disappear when stimulation is increased; these properties of secondary responses are only reproduced when NMDA receptors are located in the terminals of collateral connections. Using only rapid NMDA-independent connections, neurons in the lower layer generate a slow bell-shaped wave of excitation (a “motor command”), which is formed by sequential activation of neurons with dendritic trees of different sizes.

KEY WORDS: motor cortex, NMDA receptors, computer model.

Our previous report [4] and earlier studies described a number of neural processes which can be observed in the cat motor cortex during performance of a learned operant movement – a conditioned reflex in which the animal places its forepaw on a support. In response to a conditioned signal (electrical stimulation of the parietal cortex with trains of 3–5 impulses), the upper layers of the motor cortex demonstrate secondary, NMDA-dependent responses after the primary response. NMDA-dependent excitatory postsynaptic potentials (EPSP) with similar time parameters have been recorded intracellularly from neurons in layers II–III in cortical slices in conditions of intracortical stimulation [16]. Similar responses can be seen in the cortex after disinhibition with bicuculline and stimulation of the pyramidal tract [5]. These and other data led to the suggestion that secondary NMDA-dependent responses reflect EPSP generated in the terminals of horizontal (collateral) connections

between pyramidal neurons. From this point of view, it is understandable why the latent period of the secondary response peak (in a typical case about 70 msec, with maximum latent periods which can be greater than 100 msec – see Fig. 1 in [6]) is on average much greater than the latent period of NMDA-dependent EPSP in cortical slices (about 40 msec).

Excitatory components are most directly associated with operant movements, and these are most marked in the lower layers of the cortex and are NMDA-independent [4]. Could the neural structure of the cortex during performance of a movement response itself generate the slow wave of excitation (of duration about 300 msec) only on the basis of rapid (duration about 30 msec) NMDA-independent EPSP or could the generation of cortical “motor commands” mainly passively reflect the influx of excitation from other sources, such as the ventrolateral nucleus of the thalamus?

A more general question is that of whether and to what extent, knowing the functional characteristics of neurons and the interneuronal connections of the cortex (see, for example, [18–20]), the phenomenology of neural processes

Department of Higher Nervous Activity, M. V. Lomonosov Moscow State University. E-mail: maiorov@protein.bio.msu.ru.

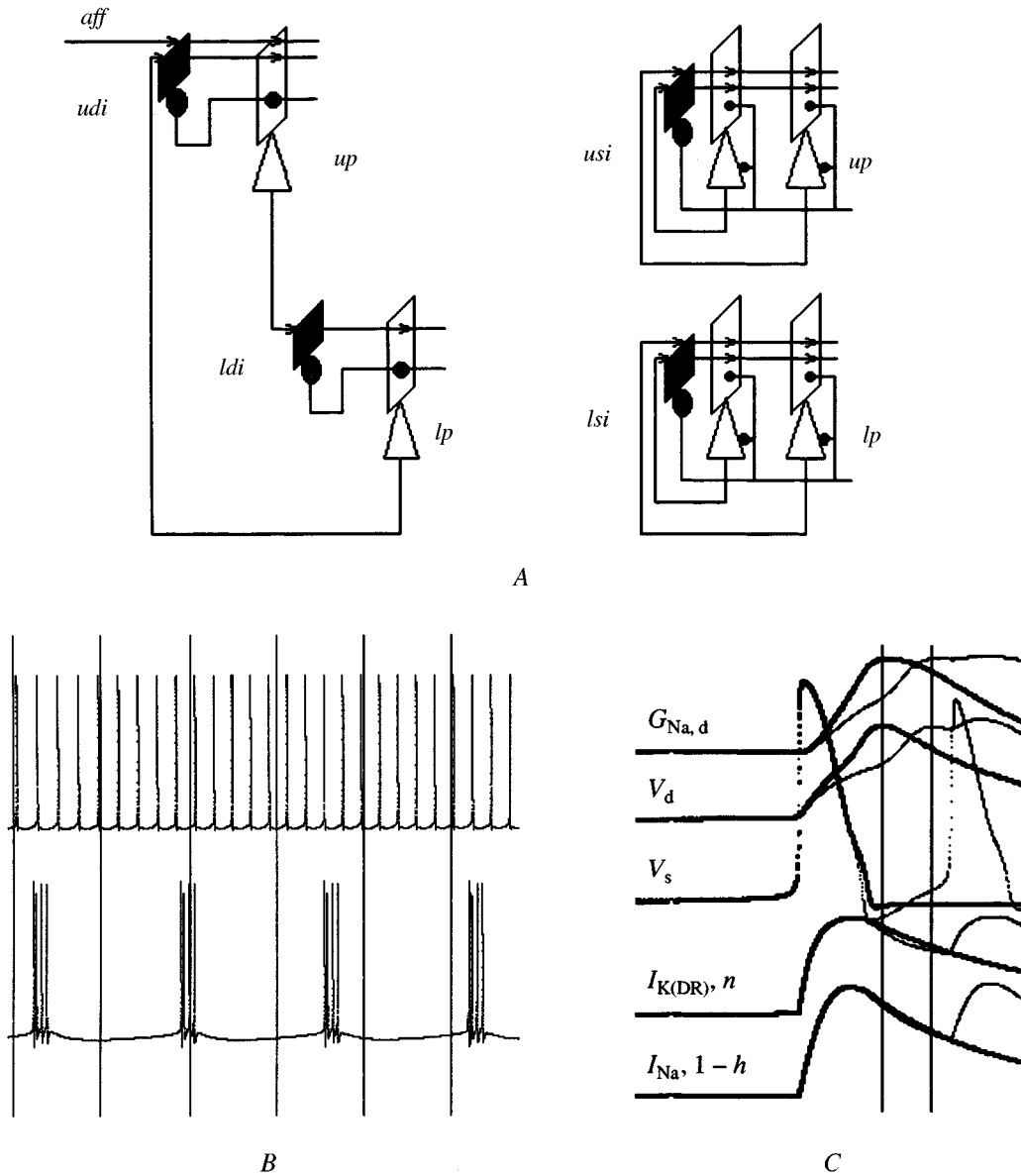


Fig. 1. Basic schemes of the model and main functional properties of individual neurons. A) Scheme of connections between neurons. Pyramidal neurons are shown as triangles and inhibitory neurons as circles. The left-hand side of the scheme shows external connections, while the right-hand side shows internal connections for each layer of the model. Afferent fibers are identified by *aff*; pyramidal (*p*) neurons of the upper (*u*) and lower (*l*) layers are identified as *up*, *lp*; interneurons (*i*) addressed to dendrites (*d*) and (in addition to dendrites) the cell body (*s*) are identified as *udi*, *ldi* and *usi*, *lsi*. All inhibitory connections (*i* →) end on GABA_A receptors. Other connections: *aff* → *up* have AMPA and NMDA receptors; *aff* → *udi* have AMPA receptors; *p* → *i* have AMPA receptors; *up* → *up* have AMPA and NMDA receptors; *up* → *lp* have AMPA and NMDA receptors; *lp* → *lp* have AMPA and NMDA receptors. The numerical parameters of neurons and connections are given in the Methods section and in figure captions. B) Activity of isolated pyramidal neurons in the upper and lower layers during passage of an intracellular current of 0.12 nA. The dendrite size of upper layer neurons is 120 times cell body size; this ratio was 160 in the lower layer. Other parameters were completely identical and are given in the Methods section. The interval between vertical lines is 100 msec. C) Fragment of the activity of upper layer neurons (thick lines) and lower layer neurons (thin lines). Traces are shifted such that the first spike in the train of the lower pyramidal cells coincided with the spike of the upper cell. $G_{Na,d}$ is the sodium conductivity in the dendritic segment; V_d and V_s are the potentials in the dendrite and cell body; n is the activation variable for the delayed rectified potassium current ($I_{K(DR)}$); h is the inactivation variable for the sodium current (this decreases during development of the action potential).

actually seen in the motor cortex during performance of an operant movement could be reproduced. Attempts to answer these questions by constructing and studying the behavior of a computer model of a cortical unit (“column”) are presented in this report.

METHODS

The model consisted of two layers of pyramidal cells (*up*, *lp* – Fig. 1, A) with two groups of inhibitory interneurons in each layer, producing direct (afferent) and inverse inhibition of pyramidal cells. The number of pyramidal cells in each layer varied from 16 to 256 in different experiments, while the number of inhibitory interneurons was always limited to one per group. The axons of pyramidal cells and direct inhibitory interneurons (marked on the diagram as *udi*, *ldi*) terminated only on dendrites, while the axons of reverse inhibitory interneurons (*usi*, *lsi*) terminated on the dendrites and bodies of target cells. The organization of interneuronal connections is shown in Fig. 1. In the prototype model, each neuron consisted of a two-segment model [15], consisting of axosomatic and dendritic segments, which provided satisfactory reproduction of many of the main functional properties of cortical pyramidal neurons. The behavior of the neuron scheme illustrated in Fig. 1 was imitated by using standard techniques for modeling neuron activity in neural structures [8, 10, 11, 13–15, 17, 21–23], which provides numerical solutions for systems of differential equations describing changes in the potential and kinetics of active ion currents in the individual segments of all neurons.

The dynamics of the potential in each segment are described by the Roll cable equation:

$$CdV/dT = -G_{\text{leak}}(V - E_{\text{leak}}) + G_{\text{in}}(V_{[-]} - V) + G_{\text{in}}(V_{[+]} - V) - (\Sigma I_{\text{syn}} + \Sigma I_{\text{m}}) + I_{\text{inj}},$$

where C is the capacitance of the membrane segment, V is the membrane potential, $V_{[+]}$ and $V_{[-]}$ are the potentials in the neighboring segments, E_{leak} is the equilibrium potential for leakage current, G_{leak} is the passive (independent of the membrane potential) leakage conductivity, G_{in} is the conductivity of the intersegmental connection (usually taken as equal to the internal longitudinal conductivity of the segment), I_{inj} is the current from the internal source injected into the cell, ΣI_{syn} is the total synaptic current summed from the various components described in detail below:

$$\Sigma I_{\text{syn}} = I_{\text{AMPA}} + I_{\text{NMDA}} + I_{\text{GABA}_A},$$

and ΣI_{m} is the sum of transmembrane ion currents, summed from several components:

$$\Sigma I_{\text{m}} = I_{\text{Na}} + I_{\text{Ca}} + I_{\text{K(DR)}} + I_{\text{K(AHP)}} + I_{\text{K(M)}} + I_{\text{K(A)}},$$

each of which is described by a Hodgkin–Huxley equation:

$$I_{\text{m}} = Ga^n b(V - E),$$

where G is the maximum conductivity for a given type of current (channel), V is the membrane potential, E is the equilibrium potential for a given ion, n is the exponent, and a and b are activation and inactivation constants, changes in which are described by kinetic equations for reversible first-order chemical reactions ($A \leftrightarrow B$):

$$dx/dt = \alpha_x(V)(1 - x) - \beta_x(V)x,$$

where x has values of a or b ; α_x and β_x are variables (at fixed potential V), their values are constant) describing the rates of the V -dependent direct ($A \rightarrow$) and reverse ($\leftarrow B$) reactions.

The functional equations and constants for all types of element in the model shown in Fig. 1 are presented below. Measurements units were: milliseconds (msec), millivolts (mV), nanoamps (nA), micrometers (μm), microsiemens (μS), megaohms ($\text{M}\Omega$), nanofarads (nF), and micromoles (μM) [23].

The common characteristics for all elements were: Faraday’s constant $F = 96484.56$, the equilibrium potential for leakage currents, individual ionic and synaptic currents $E_{\text{leak}} = -70$ mV, $E_{\text{Na}} = 50$ mV, $E_{\text{Ca}} = 140$ mV, $E_{\text{K}} = -90$ mV, $E_{\text{Cl}} = -70$ mV, $E_{\text{AMPA}} = -10$ mV, and $E_{\text{NMDA}} = -10$ mV. The resistance of connections between the somatic and dendritic segments was $R_{\text{in}} = 30 \text{ M}\Omega$, the specific conductivity of the membrane $\underline{G}_{\text{m}} = 1/3 \times 1E-6 \mu\text{S}$; and the specific capacitance was $\underline{C}_{\text{m}} = 0.75E-5$ nF [15].

Equations were then determined for individual currents and relationships between variables consisting of the rates of the direct (α) and reverse (β) reactions and the membrane potential.

The sodium current [22, 23] (m , h are the activation and inactivation variables respectively) was described by

$$I_{\text{Na}} = G_{\text{Na}} m^3 h (V - E_{\text{Na}});$$

$$\alpha_m(V) = -0.32(V + 56.9)[\exp(-(V + 56.9)/4) - 1]^{-1};$$

$$\beta_m(V) = 0.28(V + 29.9)[\exp((V + 29.9)/5) - 1]^{-1};$$

$$\alpha_h(V) = 0.128 \exp(-(V + 53)/18);$$

$$\beta_h(V) = 4[\exp(-(V + 30)/5) + 1]^{-1}.$$

The delayed rectified potassium current [22, 23] was described by

$$I_{\text{K(DR)}} = G_{\text{K(DR)}} n (V - E_{\text{K}}),$$

$$\alpha_n(V) = -0.016(V + 34.9)[\exp(-(V + 34.9)/5) - 1]^{-1};$$

$$\beta_n(V) = 0.25 \exp(-(V + 50)/40).$$

The calcium current [15] had an activation variable (s) and an inactivation variable (r):

$$I_{Ca} = G_{Ca}s^2r(V - E_{Ca});$$

$$\alpha_s(V) = 0.055(V + 27)[1 - \exp(-(27 + V)/3.8)]^{-1};$$

$$\beta_s(V) = 0.94\exp(-(V + 75)/17);$$

$$\alpha_r(V) = 4.57E - 4\exp(-(V + 13)/50);$$

$$\beta_r(V) = 0.0065[1 + \exp(-(V + 15)/28)]^{-1}.$$

The calcium-dependent potassium afterhyperpolarization current ($[Ca]$ is the internal calcium ion concentration in segments) is as described in [17] with modifications:

$$I_{K(AHP)} = GK_{(AHP)}q(V - E_K);$$

$$\alpha_q([Ca]) = 0.01([Ca]^2 - [Ca]_{Base}^2); \beta_q() = 0.02.$$

The M-type potassium current was defined as [15]

$$I_{K(M)} = G_{K(M)}u(V - E_K);$$

$$\alpha_u(V) = 1E - 4(V + 30)[1 - \exp(-(V + 30)/9)]^{-1};$$

$$\beta_u(V) = -1E - 4(V + 30)[1 - \exp((V + 30)/9)]^{-1}.$$

The A-type potassium current had an activation variable (a) and an inactivation variable (b) [22, 23]:

$$I_{K(A)} = G_{K(A)}ab(V - E_K);$$

$$\alpha_a(V) = 0.02(-56.9 - V)[\exp((-56.9 - V)/10) - 1]^{-1};$$

$$\beta_a(V) = 0.0175(V + 29.9)[\exp((V + 29.9)/10) - 1]^{-1};$$

$$\alpha_b(V) = 0.0016\exp((-83 - V)/18);$$

$$\beta_b(V) = 0.05[1 + \exp((-V - 59.9)/5)]^{-1}.$$

Changes in the synaptic conduction time were described using a double exponent method [25]:

$$G(t) = (\tau_1\tau_2/(\tau_2 - \tau_1))(\exp(-t/\tau_2) - \exp(-t/\tau_1));$$

the time to the peak was

$$t_{peak} = (\tau_1\tau_2/(\tau_2 - \tau_1))\ln(\tau_2/\tau_1);$$

the peak value was

$$G_{peak} = (\tau_1\tau_2/(\tau_2 - \tau_1))(\exp(-t_{peak}/\tau_2) - \exp(-t_{peak}/\tau_1)).$$

Channels associated with NMDA receptors have virtual conductivity, and the real (observed) conductivity depends on the membrane potential [23]:

$$G(t)_{NMDA} = G(t)_{NMDA,virt}[1 + (2/3)\exp(-0.07(V + 20))]^{-1}.$$

The time characteristics of individual synaptic currents were described by

$$\text{AMPA: } \tau_1 = 2, \tau_2 = 10, t_{peak} = 4;$$

$$\text{NMDA: } \tau_1 = 10, \tau_2 = 100, t_{peak} = 25;$$

$$\text{GABA}_A: \tau_1 = 2, \tau_2 = 10, t_{peak} = 4.$$

Allowing for the synaptic “weighting” (W), the current created by a given synapse, $I = G(t)_{eff}(V - E)$, where the “effective conductivity” $G(t)_{eff} = W(G(t)/G_{peak})$, with restrictions for the AMPA current of $G_{eff} \leq 3E-1$ and for the NMDA current $G_{eff,virt} \leq 1E-1$ [23]. Throughout the text, numerical values for synaptic efficiency are given as $(W/G_{peak}) = (G(t)_{eff}/G(t))$.

The calcium concentration within segments changes as described by [15, 17]

$$d[Ca]/dt = (-1E5/2F)(G_{Ca}s^2r(V - E_{Ca}) + G_{Ca(NMDA)}(V - E_{Ca})) - ([Ca] - [Ca]_{Base})/\tau_{[Ca]}$$

(with an additional source for Ca ion influx via NMDA channels $G_{Ca(NMDA)} = 0.03G_{NMDA}$). Since it is difficult to evaluate the volume in which ions entering cells are distributed, changes in calcium concentration $[Ca]$ are generally determined “with a precision up to the coefficient of proportionality” [8, 15, 17, 22, 23] (see, however, [12, 24]), to obtain appropriate dynamics of ion currents dependent on $[Ca]$ (here $I_{K(AHP)}$).

The specific characteristics of different types of neurons are listed below (\underline{G} is the specific conductivity, S is the surface area of a segment, ρ is the ratio of dendrite surface area to body area with subscripts identifying the axosomatic (0) and dendritic (1) segments).

Inhibitory interneurons: $\underline{G}_{0,Na} = 30000E-6$, $\underline{G}_{1,Na} = 15E-6$, $\underline{G}_{0,K(DR)} = 1500E-6$; $\underline{G}_{1,K(DR)} = 0$, $\rho = 120$, $S_0 = 100$, $S_1 = \rho S_0$.

Pyramidal neurons: baseline calcium concentration $[Ca]_{Base} = 0.1$, time constant for recovery of the calcium concentration to the initial baseline level $\tau_{[Ca]} = 200$ msec.

Upper pyramidal cells: $\rho = 120$, $S_0 = 100$, $S_1 = \rho S_0$, $\underline{G}_{0,Na} = 30000E-6$, $\underline{G}_{1,Na} = 15E-6$, $\underline{G}_{0,Ca} = 0$, $\underline{G}_{1,Ca} = 0.3E-6$, $\underline{G}_{0,K(DR)} = 1500E-6$, $\underline{G}_{1,K(DR)} = 0$, $\underline{G}_{0,K(AHP)} = 0$, $\underline{G}_{1,K(AHP)} = 2E-6$, $\underline{G}_{0,K(M)} = 0$, $\underline{G}_{1,K(M)} = 0.1E-6$, $\underline{G}_{0,K(A)} = 0$, $\underline{G}_{1,K(A)} = 0$.

Lower pyramidal cells: $\rho = 160$, $S_0 = 100$, $S_1 = \rho S_0$, $\underline{G}_{0,Na} = 30000E-6$, $\underline{G}_{1,Na} = 15E-6$, $\underline{G}_{0,Ca} = 0$, $\underline{G}_{1,Ca} =$

$= 0.3E-6$, $\underline{G}_{0,K(DR)} = 1500E-6$, $\underline{G}_{1,K(DR)} = 0$, $\underline{G}_{0,K(AHP)} = 0$,
 $\underline{G}_{1,K(AHP)} = 2E-6$, $\underline{G}_{0,K(M)} = 0$, $\underline{G}_{1,K(M)} = 0.1E-6$, $\underline{G}_{0,K(A)} = 0$,
 $\underline{G}_{1,K(A)} = 0$.

The relative size of dendrites (ρ) and the synaptic conductivity (\underline{G}) for individual types of connection were selected randomly from a normal distribution with a specified mean and dispersion. Negative weightings or connections, which could occur as a result of this method, were replaced with zero.

The program was written in C++ in the visual programming environment Borland C++ Builder 4. Numerical solutions of the complete system of differential equations describing the behavior of the model were obtained by the Rung–Kutt–Felberg method with a variable step [1, 2, 7].

RESULTS

Figure 1, *B* shows an example of the activity of two pyramidal neurons, one in the upper and one in the lower layer of the model, isolated from all synaptic connections, in conditions of an identical transmembrane current $I_{inj} = 0.12$ nA. All neuron parameters were completely identical apart from dendrite size, which was $120S_0$ ($1.2E5 \mu\text{m}^2$) for the upper layer pyramidal cell and $160S_0$ ($1.6E5 \mu\text{m}^2$) for the lower layer pyramidal cell. This reproduces the result obtained in [15] and showed that the regime in which the pyramidal cell operates (trains, or regular firing) may be determined only by the relative (to the body) size of the dendritic tree. Figure 1, *C* allows identification of why trains are generated. After generation of the preceding somatic spike, the potential in the dendrite of the lower pyramidal cells (thin lines) reaches a peak later than the potential in the dendrite of the upper cell (thick lines), when inactivation of the sodium current and potassium permeability in the cell body are already relatively weak and allow generation of an additional spike because of dendritic depolarization triggered in the cell body.

Figure 2 shows examples of the responses of a group of pyramidal cells in the upper layer of the model in response to a train of spikes in the afferent fiber. The response consists of primary and secondary excitatory components; the latent period of the secondary response in fragments *B* and *D* corresponds to the maximum values seen in experimental conditions (see, for example, Fig. 1 in [6]). In agreement with experimental data, secondary responses appear in conditions of reduced GABA_A-dependent inhibition (Fig. 2, *B*). Analysis of changes in synaptic conductivity included in the model neurons allows us to follow the chain of events leading to generation of the secondary response. Minimal weakening of inhibition at the start of the response (decreased GABA_A conductivity in Fig. 2, *B* as compared with that in Fig. 2, *A* is colored black) has the result that some additional neurons generate spikes in response to afferent stimulation; this increases the “reserve”

of virtual NMDA conductivity (nmda, the increase in conductivity corresponding to the white space between curves) accumulating in the dendrite membrane. If the residual virtual NMDA conductivity is quite high after the end of the GABA_A current, as shown in Fig. 2, *B*, then a secondary response can be generated. Increased stimulation (reflected as an increase in primary responses) leads to disappearance of secondary responses (Fig. 2, *C*) because of an increase in afterhyperpolarization, $I_{K(AHP)}$. A slight weakening of $I_{K(AHP)}$ is sufficient for restoration of secondary responses (Fig. 2, *D*). Weakening of the NMDA current leads to disappearance of secondary responses (Fig. 2, *E*). An increase in NMDA conductivity, along with changes in a number of other parameters in Fig. 2, *F*, leads to a significant shortening of the latent period of the secondary response. The lower part of the figure shows a histogram of the distribution of averaged secondary responses generated in this test by all neurons in the model superimposed with histograms of several typical secondary responses recorded in real experiments (the lower fragment of the figure is reproduced, with a scale change, from Fig. 1, *A* from [4]).

Figure 3 shows the generation of secondary responses when NMDA receptors are located not in the terminals of the reverse collaterals of pyramidal neurons (as shown in the diagram and the examples presented in Fig. 2), but in the terminals of the afferent fibers on the dendrites of pyramidal cells. However, with NMDA receptors in this disposition, the relationship between secondary responses and the strength of afferent inhibition did not correspond to that observed experimentally. Secondary responses appeared when the strength of afferent inhibition was increased and paralleled a decrease in primary responses (Fig. 3, *B*); further increases in inhibition caused primary response to disappear, while secondary responses increased and showed reductions in their latent period (Fig. 3, *C, D*). Thus, this situation did not yield the effect characteristic of cerebral cortex neurons, whereby secondary responses appear in conditions of suppression of GABA_A-dependent inhibition; conversely, secondary responses appear not in conditions of weakening but in conditions of strengthening of GABA_A inhibition.

Figure 4, *A* shows the generation of “motor commands” by neurons in the lower layer of the model, influenced by the source of activity in the upper layer. “Rapid” collateral EPSP of the non-NMDA type were required for generation of a wave of excitation in the lower layer, and the duration of this significantly exceeded the duration of individual EPSP. In fragment *B*, the histogram showing the overall response generated by pyramidal neurons of the lower layer of the model (thick line) is compared with a histogram of the electromyographic response of elbow flexion in a cat during rapid performance of the paw-placing conditioned reflex (thinner line). A significant characteristic of the morphology of the lower layer of the model is that different neurons have dendritic trees of different sizes. In

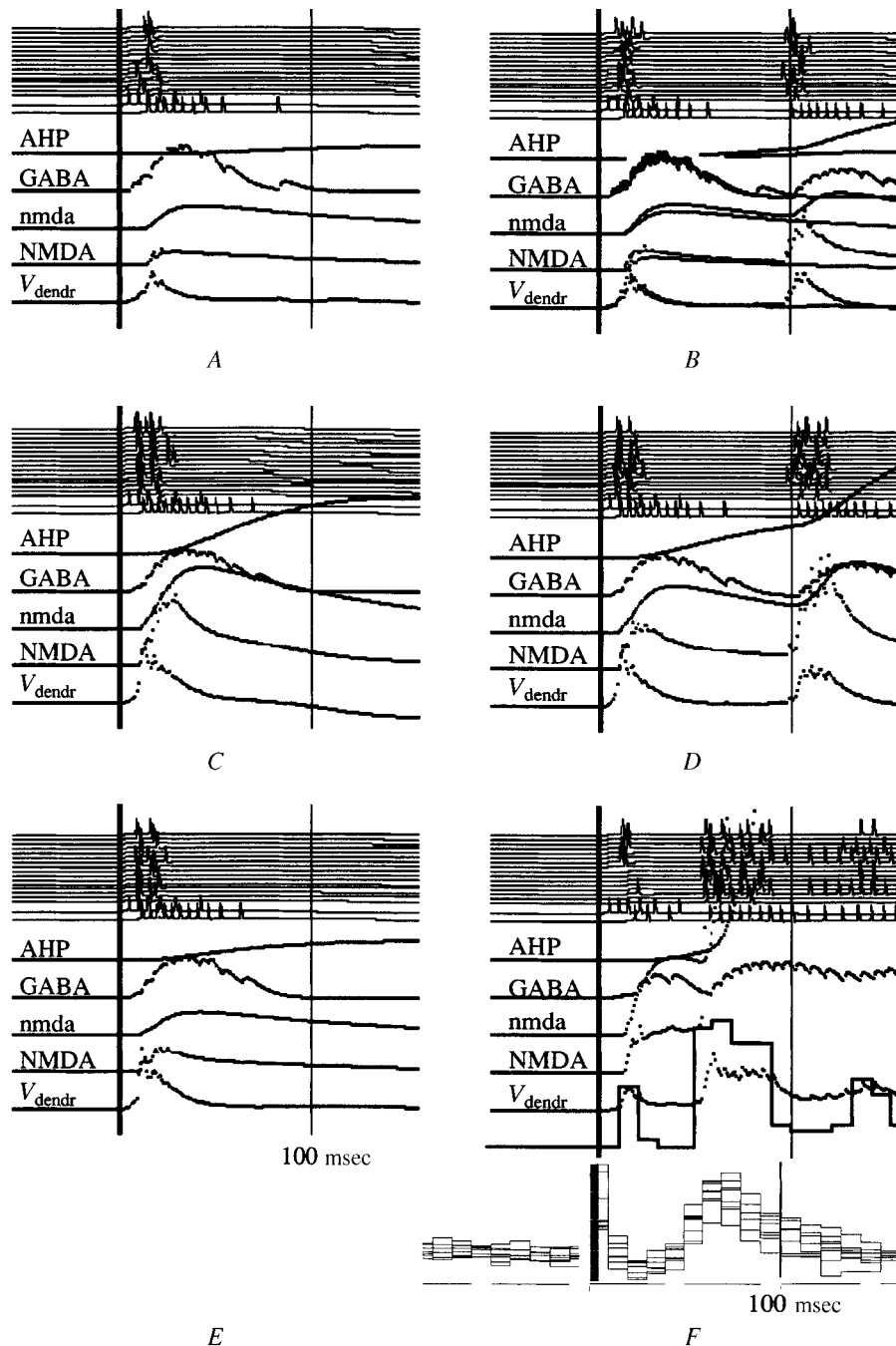


Fig. 2. Responses of pyramidal cells in the upper layer ($n = 16$) to a train of three spikes with interspike intervals of 3 msec generated by one afferent fiber branching to all the pyramidal cells of the upper layer and an interneuron on the direct inhibitory pathway (*udi*). The first spike in the train corresponds to the thick vertical line in the figure. The upper part of each fragment shows the spike activity of the pyramidal cells and two inhibitory neurons (the last two rows); the lower part shows changes (averaged for all the pyramidal cells) in conductivity and potential in the dendritic segment (AHP = $G_{K(AHP)}$); GABA = G_{GABA} ; nmda = the virtual and NMDA the real conductivity of channels associated with NMDA receptors; V_{dendr} = potential of the dendritic segment (see Methods section). Changes in conductivity and potential in examples A and B are lined up with fragment B. Light and dark intervals between curves show areas in which the curves from fragment B are, respectively, higher and lower than the curves in fragment A. Neuron and connection parameters differing from those given in the Methods section were: A) $\rho = 100 \pm 20$; $G_{1,K(AHP)} = 3E-6$; $aff \rightarrow up_{1,AMPA} = 0.25 \pm 0.2E-3$; $aff \rightarrow up_{1,NMDA} = 0$; $aff \rightarrow udi_1 = 4E-3$; $up \rightarrow up_{1,AMPA} = 0.75 \pm 0.5E-3$; $up \rightarrow up_{1,NMDA} = 0.15 \pm 0.1E-3$; $up \rightarrow usi_1 = 2E-3$; $udi \rightarrow up_1 = 0.9E-2$; $usi \rightarrow up_0 = 1.2E-2$; $usi \rightarrow up_1 = 0.9E-2$. B) (differing from A): $udi \rightarrow up_1 = 0.5E-2$. C) (differing from B): $aff \rightarrow up_{1,AMPA} = 0.75 \pm 0.2E-3$. D) (differing from C): $G_{1,K(AHP)} = 1.5E-6$. E) (differing from D): $up \rightarrow up_{1,NMDA} = 0.0 \pm 0.1E-3$. F) (differing from A): half the neurons (0–7) had $aff \rightarrow up_{1,AMPA} = 0.3 \pm 0.05E-3$, the others (8–15) had 0; $up \rightarrow up_{1,AMPA} = 0.1 \pm 0.05E-3$; $up \rightarrow up_{1,NMDA} = 0.75 \pm 0.05E-3$; $up \rightarrow usi_1 = 0.4E-3$; $usi \rightarrow up_{0,1} = 1.25E-2$; $udi \rightarrow up_1 = 0.2E-2$. The lower part of fragment F shows averaged post-stimulus histograms of all the pyramidal neurons of the model in this trial with superimposition of real neuron responses in the cat motor cortex (from Fig. 1, A in [4]).

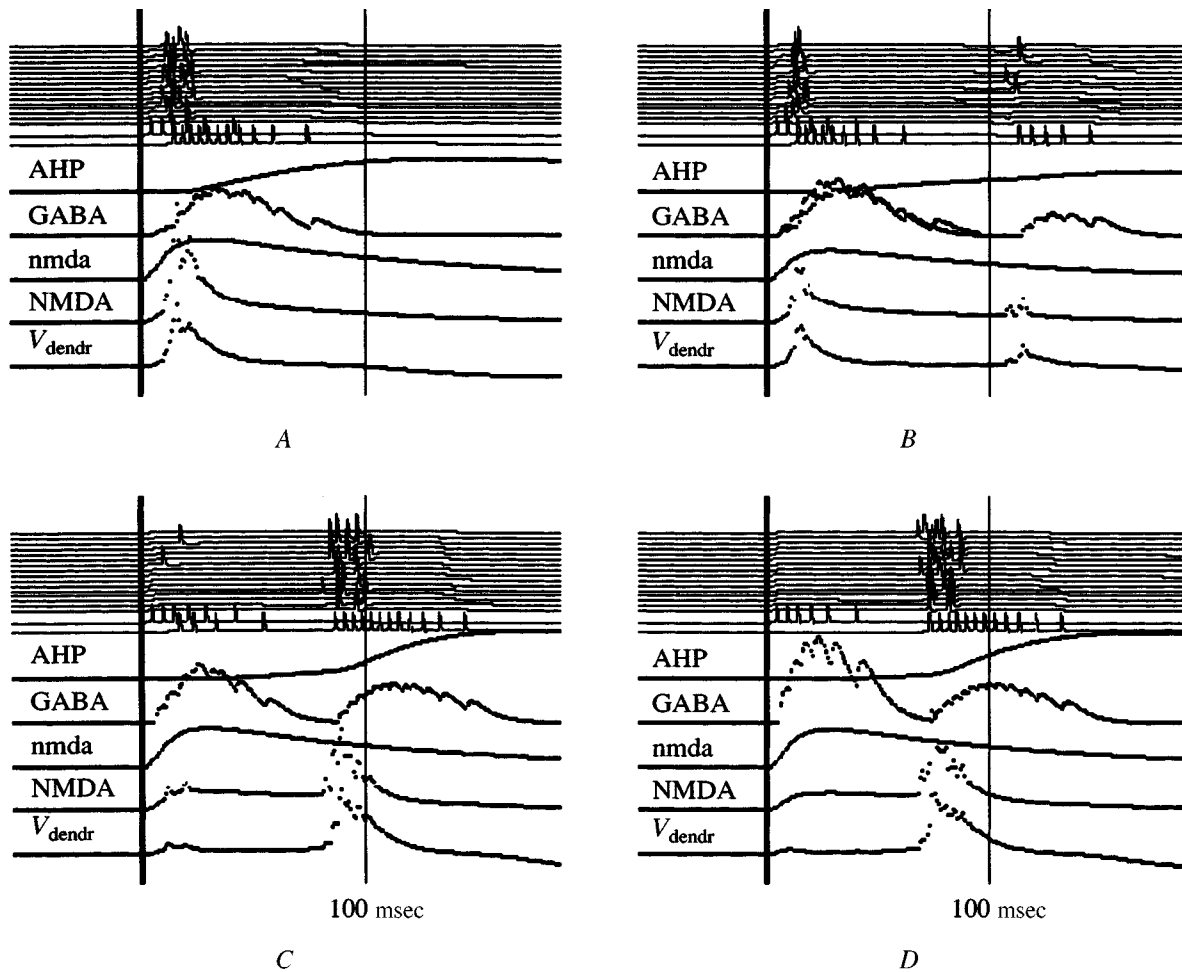


Fig. 3. Changes in the characteristics of secondary responses when NMDA receptors are moved from the terminals of collateral connections to afferent endings on pyramidal neurons. Abbreviations are as in Fig. 2. Only the characteristics of connections differing from those in the example in Fig. 2, *B* are shown. *A*) $aff \rightarrow up_{1,AMPA} = 0.25 \pm 0.5E-3$; $aff \rightarrow up_{1,NMDA} = 1 \pm 0.5E-3$; $up \rightarrow up_{1,NMDA} = 0$; $udi \rightarrow up_1 = 0.5E-2$. *B*) (Differing from Fig. 3, *A*): $udi \rightarrow up_1 = 1.0E-3$. *C*) $udi \rightarrow up_1 = 1.5E-3$. *D*) $udi \rightarrow up_1 = 3.0E-3$.

Fig. 4, *A*, the neurons are ordered by size, such that the top curve corresponds to the neuron with the smallest dendritic tree and the bottom curve shows the neuron with the largest dendritic tree. The neurons are activated sequentially, and those neurons which are excited earlier also fall silent earlier. This is the type of involvement observed in the activity of real neurons in the cat motor cortex during performance of the conditioned reflex movement (Fig. 4, *C*).

Figure 4, *D*, *E* shows how the responses of neurons in the lower layer of the model change with changes in the mean value of the descending (from neurons in the upper layer) and horizontal (between neurons in the lower layer) connections. The initial response corresponded to curve 1 on both plots. Weakening of the descending (curve 3) or collateral (curve 2) excitatory connections in the lower layer led to increases in the latent period of generation of the wave of excitation. However, these methods of changing the latent period did not have identical effects: changes in

the strength of the descending (external from the point of view of neurons in this layer) connections did not alter the shape of the leading front of the wave of excitation (from the start to the peak) (Fig. 4, *D*, *E*, 1, 3, while essentially the same changes in latent period due to weakening of internal horizontal connections resulted in a slower development of the response (with a more gently sloping leading front) (Fig. 4, *D*, *E*, 1, 2).

Figure 5 shows the effects of the extent of activation from the upper layer and the intrinsic state of pyramidal neurons in the lower layer on the generation of the wave of excitation by neurons in the lower layer. In this case, pyramidal neurons of the upper layer are divided into two groups of eight neurons (neurons 0–7 and 8–15, numbered from above downwards). Excitatory collateral connections of the NMDA type between neurons within each group were stronger than those between neurons belonging to different groups (connection strengths are shown in the cap-

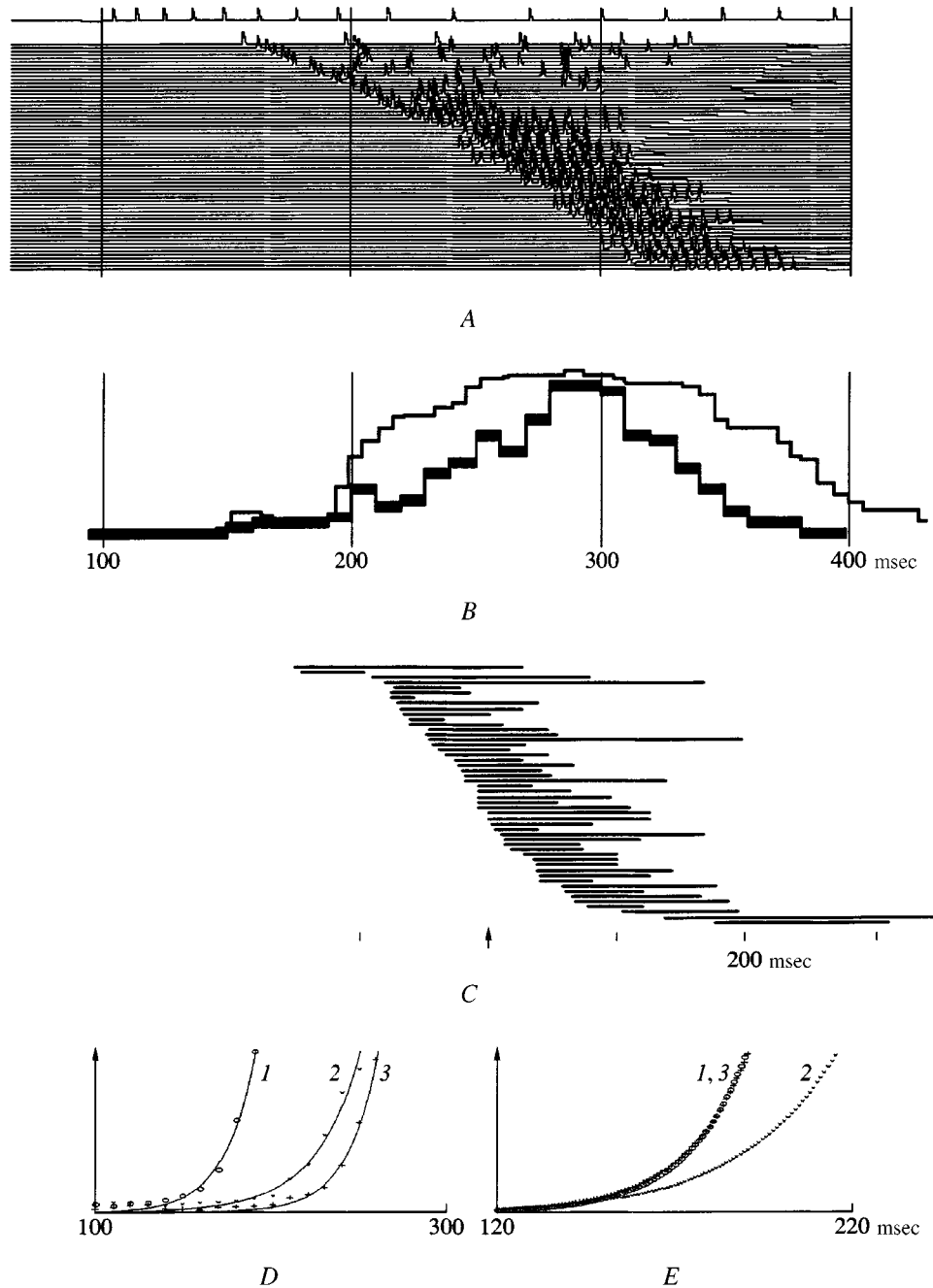


Fig. 4. Characteristics of the activity of different neurons in the model during the process of generating a "motor command." *A*) Generation of a wave of excitation by pyramidal neurons in the lower layer, consisting of 64 neurons, in response to the activity of one upper layer pyramidal neuron induced by intracellular depolarization (a current of 0.05 nA during the interval from 0 to 100 msec, 0.15 nA from 100 msec to the end of the analysis epoch). Timing is shown relative to the beginning of the analysis epoch. Neurons are ordered by the size of their dendritic segments. Neuron and connection parameters: $up: \rho = 120; \underline{G}_{1,K(AHP)} = 3E-6; up \rightarrow usi_1 = 2E-3; up \rightarrow ldi_1 = 1E-3; up \rightarrow lp_{1,AMPA} = 0.25E-4; up \rightarrow lp_{1,NMDA} = 2E-4; usi \rightarrow up_0 = 1.2E-2; usi \rightarrow up_1 = 0.9E-2; lp: \rho = 100 + 3i$, where i is the neuron identification number (0–63); $\underline{G}_{1,K(AHP)} = 0.5E-6; lp \rightarrow lp_{1,AMPA} = 0.075 \pm 0.05E-4; lp \rightarrow lp_{1,NMDA} = 0; lp \rightarrow lsi_1 = 0.75E-4; ldi \rightarrow lp_1 = 2E-3; lsi \rightarrow lp_0 = 1E-4; lsi \rightarrow lp_1 = 1E-4; lp \rightarrow up_{1,AMPA} = 0; lp \rightarrow up_{1,NMDA} = 0$. *B*) Overall histogram of the activity of pyramidal neurons in the lower layer of the model (thick line) and histogram of electromyogram responses from the forelimb biceps of a cat during performance of the conditioned paw-placing reflex (thin line, from Fig. 29, A, 1 in [3]). *C*) Distribution of the periods of maximum neuron activity in the cat motor cortex during performance of the conditioned paw-placing reflex (from Fig. 35 in [3]) relative to the onset of movement (the arrow shows the moment at which the half-maximal biceps electromyogram value is reached in each response). *D*) Increase in the latent period of the wave of excitation in the lower layer relative to the initial position (1) in conditions of weakened descending (3) and collateral (2) connections. Exponents are shown for the last five points of each response, corresponding to the leading front of the wave of excitation. Time is indicated relative to the beginning of the analysis epoch. *E*) Displacement of the exponent from Fig. 4, *D* (relative to the initial response, shown as circles). In conditions of constant collateral connections between pyramidal neurons in the lower layer, despite the larger difference in latent periods, approximation exponentials for the leading fronts of the excitation wave coincided precisely (1, 3), while changes in collateral connections cause them to diverge (2).

tion to the figure). Neurons were activated by passage of short (10 msec) depolarizing currents through neurons 0–2 and 14–15. Secondary responses and subsequent excitation were generated only by the second group of neurons. Figure 5, A shows an example of the generation of a motor command in the lower layer of the model under the influence of activation of a group of neurons in the upper layer (neurons of the lower layer were ordered in terms of the size of the dendritic tree, as in Fig. 4, A). It is evident that generation of the wave of excitation in the lower layer induces additional excitation of upper layer neurons due to ascending excitatory collaterals from the lower layer to the upper. The wave of excitation in the lower layer did not appear after slight decreases in the responses of upper layer neurons were induced by 10% weakening of collateral connections between pyramidal neurons (Fig. 5, B). The inclusion of potassium A-currents into the model of lower layer pyramidal neurons blocked generation of the motor command when the strength of collateral connections in the lower layer was doubled (Fig. 5, C).

DISCUSSION

Mechanism of Train Generation. Previous studies [15] showed that the activity regime of pyramidal neurons can be determined by a single parameter – the size of the dendrite as a proportion of the size of the cell body; this result was reproduced in the present work and is shown in Fig. 1. The authors of [15] restricted their evidence to the point that the generation of trains requires the presence of a small level of sodium conductivity in the dendrite. There are therefore grounds to consider the mechanism of origination of trains in more detail.

1. $V_{\text{dendr}} \rightarrow V_{\text{body}}$. Generation of EPSP in the dendrite induces propagation of a wave of depolarization towards the cell body, where an action potential is generated when the critical level of depolarization is reached. (In the case shown in Fig. 1, depolarization of the body is due immediately to passage of the intracellular current.)

2. $V_{\text{body}} \rightarrow V_{\text{dendr}}$. Depolarization of the cell body induced by the action potential propagates back to the dendrite and charges the dendritic capacitance (C_{dendr}) via a longitudinal resistance (in the model this is R_{in} , linking the somatic segment with the dendritic segment) with a time constant of $\tau = R_{\text{in}}C_{\text{dendr}}$.

3. $V_{\text{dendr}} \rightarrow V_{\text{body}}$. This depolarization leads to activation of the dendritic sodium conductivity, which increases the depolarization of the dendrite (producing a dendritic spike); the enhanced depolarization wave returns to the cell body.

4. The following events depends on which state the cell body is in when excitation returns from the dendrite. If excitation from the dendrite returns rapidly, it arrives during the refractory period of its parent spike and disappears. If the

dendritic excitation is delayed, it can induce an additional offspring spike in the cell body and initiate generation of a train. If we ignore the effect of the transmembrane leakage current, then the delay time depends on the time constant for charging the dendritic capacitance ($\tau = R_{\text{in}}C_{\text{dendr}}$). The delay increases with increases in the area and electrical capacitance of the dendrite (C_{dendr}) and internal transfer resistance (R_{in}), which are determined by the morphology of the neuron. However, the transverse (active) conductivity of the dendrite membrane is variable (for example, the total level of potassium conductivity is controlled by neuromodulators). This mechanism allows the regime of neuron activity to be controlled functionally (for example, replacement of regular train activity during the transition from waking to sleep).

Mechanism of Generation of Secondary Responses.

The model shows that the generation and time parameters of secondary responses are determined by the magnitude and dynamics of GABA_A- and NMDA-dependent synaptic conductivities and the calcium-dependent potassium current ($I_{\text{K(AHP)}}$) respectively. Secondary responses are generated because of the “residual” virtual NMDA conductivity, which persists to the end of the GABA_A current. This mechanism, in particular, explains the fact that being NMDA dependent, secondary responses peak significantly later than NMDA-dependent EPSP. The model reproduces the main properties of secondary responses – their appearance and enhancement in conditions of suppression of GABA_A-dependent inhibition and their disappearance when stimulation is increased – due to the development of afterhyperpolarization ($I_{\text{K(AHP)}}$). Weakening of afterhyperpolarization (for example, because of increases in the total level of “arousal”) leads to the appearance and enhancement of secondary responses. An unexpected result from observing the behavior of the model was that the properties of secondary responses depended on the location of NMDA synapses. Secondary responses appeared and were enhanced in conditions of suppression of GABA_A inhibition only when NMDA synapses were located on the reverse terminals of pyramidal cell axons. If these synapses were located at the site of the endings of corticocortical afferent axons, then the secondary responses generated in this situation only weakened when GABA_A-dependent inhibition decreased. The point is that in the first case, activation of collateral EPSP required a certain number of pyramidal neuron discharges, while in the second case (when membrane depolarization alone was sufficient to activate NMDA conductivity), the effect of spike generation on the generation of NMDA EPSP is exclusively negative, consisting of induction of post-spike afterhyperpolarization. This result provides further support for the hypothesis that secondary responses have collateral origination [5].

Mechanism of Generation of the “Motor Command.” Generation of the “motor command” in the model shows significant but not obvious similarities with the real

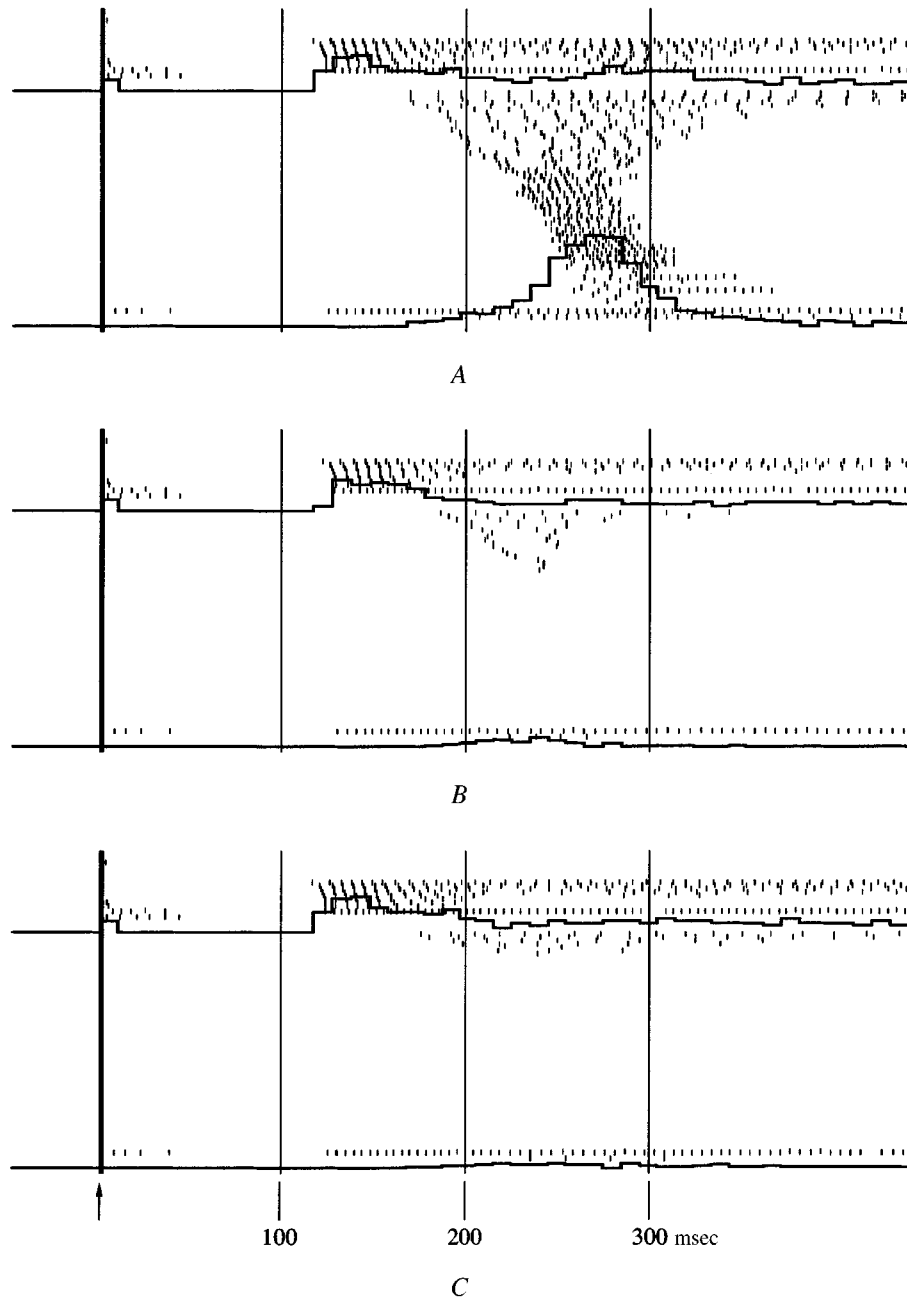


Fig. 5. Conditions for generation of a "motor command" by pyramidal neurons in the lower layer of the cortex. *A*) Generation of a wave of excitation in the lower layer ($n = 64$) in response to activity of pyramidal neurons in the upper layer ($n = 16$) induced by passage of a spike of intracellular depolarizing current of 0.1 nA during the time period 0–10 msec via pyramidal neurons 0–2, 14, and 15 and over the time period 0–50 msec via the direct inhibitory interneuron (*udi*). The moment at which the current was started is indicated by the arrow and the thick vertical line. The upper and lower histograms in each figure show the total numbers of spikes generated in 10 msec by all pyramidal neurons in the upper and lower layers. Pyramidal neurons of the upper layer were divided into two groups of eight neurons (0–7 and 8–15); parameters of the connections between neurons within each group were: $up \rightarrow up_{1,AMPA} = 0.5E-4$; $up \rightarrow up_{1,NMDA} = 1.2E-3$; parameters of intergroup connections were: $up \rightarrow up_{1,AMPA} = 0.5E-4$; $up \rightarrow up_{1,NMDA} = 1.2E-4$; other parameters (differing from Fig. 4, *A*) were: $up: \rho = 80 + 8i$ ($i < 8$), $\rho = 80 + 8(i - 8)$ ($i \geq 8$); $G_{1,K(AHP)} = 3E-6$; $up \rightarrow lp_{1,AMPA} = 0.1E-4$; $up \rightarrow lp_{1,NMDA} = 0.4E-4$; $udi \rightarrow up_1 = 2E-1$; $lp: p = 200 \pm 100$; $lp \rightarrow lp_{1,AMPA} = 0.11 \pm 0.11E-4$; $lp \rightarrow lsi_1 = 0.7E-4$; $ldi \rightarrow lp_1 = 3.1E-3$; $lp \rightarrow up_{1,AMPA} = 0.2E-4$. *B*) Absence of wave of excitation in the lower layer when excitation of upper layer neurons was reduced. Intragroup connections in the upper layer for AMPA and NMDA receptors: $up \rightarrow up = 1.1E-3$. *C*) Blockade of generation of a motor command in the lower layer after addition of K(A)-type conductivity to pyramidal cells of the lower layer, $G_{1,K(A)} = 0.5E-5$; $lp \rightarrow lp_{1,AMPA} = 0.22 \pm 0.11E-4$. Neuron activity rasters show overall histograms for pyramidal cells in the upper and lower layers separately. The first stimulus spike in the train corresponds to the thick vertical line and the arrow.

process in the motor cortex. Qualitatively, this applies to the nature of involvement, i.e., sequential periods of activation, of different neurons in the motor cortex which is seen during performance of the conditioned paw-placing reflex [3]. It can be seen from the comparison shown in Fig. 4, *A* and *B* that the range of involvement of the cortex is about twice as wide as that of the model (the scale in Fig. 4, *C* is twice that of Fig. 4, *A*, *B*). One reason for this may be the method used for determining the periods of maximum neuron activity in Fig. 4, *C*, from *averaged* post-stimulus histograms; the width of the averaged response increases because of the performance of individual movements with different latent periods. Comparison of the wave of excitation generated by the model with the dynamics of the most rapidly performed operant movements, as shown in Fig. 4, *B*, demonstrates good agreement of the overall dynamics of the responses in both cases. The sequential involvement of neurons in the wave of excitation depends on the dispersion of the sizes of the model nerve cells. Over a particular range, an increase in dispersion leads to an increase in the duration of the excitation wave generated. The sequential activation effect is based on the ability of large neurons in the lower layers to generate train activity. In comparison with neurons in the upper layer, neurons in the lower layer showed a decreased extent of afterhyperpolarization ($G_{K(AHP)}$); otherwise, trains would be interrupted too quickly in conditions of a high initial spike frequency, because of rapid increases in the Ca-dependent potassium current. This effect, which was seen only because of the difference in the morphological sizes of individual nerve cells, may apparently appear (or strengthen) because of the spread in the functional parameters, for example, the magnitudes of potassium currents.

The shape of the leading front of the “motor command” in the model remained constant despite significant changes in the latent period induced by changes in the external influx to the neurons of the lower layer generating the “motor command” (with no change in the efficiency of the connections between them). This characteristic effect has also been seen in a number of experimental studies. In real conditions, the shape of the “motor component” of the responses of cortical neurons is not dependent on the nature of the triggering conditioned signal [3]. Functional exclusion of the cerebellar nuclei [9] induced sharp increases in the latent period of the movement-associated wave of excitation in the motor cortex without change in its shape and size.

Why the “Motor Command” is Generated. In the model, the motor cortex appears to display excessive independence, generating the “motor command” without “authorization” from outside. The “authorizing” mechanism may result, for example, from the action of neurotransmitters facilitating more effective external activation or interaction of generator neurons during the process of formation of the “motor command.” This, in particular, shows that the effective target for neurotransmitters may be den-

dritic conductivity of the K(A) type, activation (or strengthening) of which can be blocked by generation of the “motor command” in the cortex.

CONCLUSIONS

Computer modeling showed that the neural structures in which the properties of individual elements and the scheme of connections between them correspond to the real characteristics of the neural structure of the cerebral cortex and reproduce the main forms of activity seen in real physiological experiments on the performance of an operant movement. Pyramidal neurons in the upper layer generated primary and secondary responses to external stimulation. As in real experiments, secondary NMDA-dependent responses appeared in conditions of weakening of GABA_A inhibition and disappeared when stimulation increased; these properties of secondary responses were reproduced only when NMDA receptors were located in the terminals of collateral connections. When all connections were of the rapid, NMDA-independent type, neurons in the lower layer generated a slow bell-shaped wave of excitation (a “motor command”), which formed as a result of sequential activation of neurons with dendritic trees of different sizes.

We would like to thank the editors for identifying inaccuracies and an error in the equation describing the calcium current through NMDA channels.

This study was supported by the Russian Fund for Basic Research (Grant No. 99-04-49350).

REFERENCES

1. V. P. D'yakonov, *Handbook of Algorithms and Programs in BASIC for Personal Computers* [in Russian], Nauka, Moscow (1989).
2. D. Kachander, K. Moular, and S. Nesch, *Numerical Methods and Programming* [Russian translation], Mir, Moscow (1998).
3. B. I. Kotlyar, V. I. Maiorov, N. O. Timofeeva, and V. V. Shul'govskii, *Neuronal Organization of Conditioned Reflex Behavior* [in Russian], Nauka, Moscow (1983).
4. V. I. Maiorov, “NMDA-dependent and NMDA-independent neuronal processes in the bicuculline-disinhibited motor cortex of the cat during the acquisition and reproduction of a paw-placing reflex,” *Zh. Vyssh. Nerv. Deyat.*, **52**, No. 2, 205 (2002).
5. V. I. Maiorov, “Late excitatory responses of neurons in the cat motor cortex to stimulation of the pyramidal tract,” *Zh. Vyssh. Nerv. Deyat.*, **51**, No. 1, 316 (2001).
6. V. I. Maiorov and A. A. Moskvitin, “Long-term potentiation of the late NMDA-dependent component of cat motor cortex neuron responses to stimulation of the direct cortical input from field 5 of the parietal cortex,” *Zh. Vyssh. Nerv. Deyat.*, **49**, No. 2, 279 (1999).
7. D. MacCracken and U. Dorn, *Numerical Methods and Programming in Fortran* [Russian translation], Mir, Moscow (1977).
8. E. Barkai and M. E. Hasselmo, “Modulation of the input-output function of rat piriform cortex pyramidal cells,” *J. Neurophysiol.*, **72**, No. 2, 644 (1994).
9. V. B. Brooks, J. Adrien, and R. W. Dykes, “Task-related discharge of neurons in motor cortex and effects of dentate cooling,” *Brain Res.*, **40**, No. 1, 85 (1972).

10. P. C. Bush and T. J. Sejnowski, "Reduced compartmental models of neocortical pyramidal cells," *J. Neurosci. Meth.*, **46**, 159 (1993).
11. E. Fransen, *Biophysical Simulation of Cortical Associative Memory*, Dissertation, University of Stockholm (1996).
12. H. J. Koestler and B. Sakmann, "Calcium dynamics in single spines during coincident pre- and postsynaptic activity dependent on relative timing on back-propagating action potentials and subthreshold excitatory postsynaptic potentials," *Proc. Natl. Acad. Sci. USA*, **95**, 9596 (1998).
13. W. W. Lytton and T. J. Sejnowski, "Simulations of cortical pyramidal neurons synchronized by inhibitory interneurons," *J. Neurophysiol.*, **66**, No. 3, 1059 (1991).
14. Z. F. Mainen, J. Joerges, J. R. Huguenard, and T. J. Sejnowski, "A model of spike initiation in neocortical pyramidal neurons," *Neuron*, **15**, 1427 (1995).
15. Z. F. Mainen and T. J. Sejnowski, "Influence of dendritic structure of firing pattern in model neocortical neurons," *Nature*, **382**, 323 (1996).
16. B. Sutor and J. J. Hablitz, "EPSPs in rat neocortical neurons in vitro. I. Electrophysiological evidence for two distinct EPSPs," *J. Neurophysiol.*, **61**, No. 3, 607 (1989).
17. A. C. Tang, A. M. Bartels, and T. J. Sejnowski, "Effects of cholinergic modulation on responses of neocortical neurons to fluctuating input," *Cerebral Cortex*, **7**, No. 6, 502 (1997).
18. A. M. Thomson, "Facilitation, augmentation and potentiation at central synapses," *Trends Neurosci.*, **23**, 305 (2000).
19. A. M. Thomson and J. Deuchars, "Temporal and spatial properties of local circuits in neocortex," *Trends Neurosci.*, **17**, No. 3, 119 (1994).
20. A. M. Thomson and J. Deuchars, "Synaptic interactions in neocortical local circuits: dual intracellular recordings in vitro," *Cerebral Cortex*, **7**, No. 6, 510 (1997).
21. R. D. Traub, "Simulation of intrinsic bursting in CA3 hippocampal neurons," *Neurosci.*, **7**, No. 5, 1233 (1982).
22. R. D. Traub, J. G. R. Jeffreys, R. Miles, et al., "A branching dendritic model of a rodent CA3 pyramidal neurone," *J. Physiol.*, **481**, 79 (1994).
23. R. D. Traub, R. K. S. Wong, R. Miles, and H. Michelson, "A model of a CA3 hippocampal pyramidal neuron incorporating voltage-clamp data on intrinsic conductances," *J. Neurophysiol.*, **66**, No. 2, 635 (1991).
24. R. Yuste, A. Majewska, S. S. Cash, and W. Denk, "Mechanisms of calcium influx into hippocampal spines: heterogeneity among spines, coincidence detection by NMDA receptors and optical quantal analysis," *J. Neurosci.*, **19**, No. 6, 1976 (1999).
25. M. Wilson and J. M. Bower, "Cortical oscillations and temporal interactions in a computer simulation of piriform cortex," *J. Neurophysiol.*, **67**, No. 4, 981 (1992).